

# Radiation Treatment in the GISS GCM

A. A. Lacis, V. Oinas, and B. Cairns  
 NASA-Goddard Institute for Space Studies  
 New York, New York

## Introduction

The primary role of radiative transfer calculations in climate general circulation models (GCMs) is to provide accurate heating and cooling rates for the radiative energy terms in the fundamental equations. A secondary role is to represent GCM physical processes in terms of radiative quantities that can be effectively compared to satellite and ground-based observational data.

## Solar Radiation

The gaseous absorbers included in the Goddard Institute for Space Studies (GISS) GCM are H<sub>2</sub>O, CO<sub>2</sub>, O<sub>3</sub>, O<sub>2</sub>, and NO<sub>2</sub>, utilizing 15 spectrally noncontiguous, vertically correlated k-distribution intervals. Cloud and aerosol radiative parameters (extinction cross-section, single scattering albedo, and asymmetry parameter) are calculated using Mie theory with compensation for nonspherical effects for dust and ice clouds (Lacis and Mishchenko 1995).

Multiple scattering of solar radiation utilizes the doubling/adding method (Lacis and Hansen 1974) with single Gauss point (SGP) adaptation to reproduce the solar zenith angle dependence for reflected solar radiation by clouds and aerosols with the same degree of precision as the full doubling-adding for conservative scattering (Figure 1a). This is achieved by means of a brute-force look-up table in  $\tau, g, \mu_0$ , which returns an "effective" asymmetry parameter value,  $g'$ , to be used in the SGP doubling algorithm to reproduce the correct albedo. Otherwise, the commonly used two-stream type multiple scattering models produce albedo errors that are about 10% depending on the optical depth, solar zenith angle, and scattering phase function (King and Harshvardhan 1986).

Errors arise in multilayered atmospheres, when the conservative scattering layer in Figure 1a is added on top of a strongly reflecting Lambertian surface of albedo 0.5. Though not very large in the first place, these errors also integrate out to near-zero during the course of a day. Nevertheless, a 3% albedo overestimation at high sun coupled with a 3% underestimation at low sun could act to produce a diurnal bias.

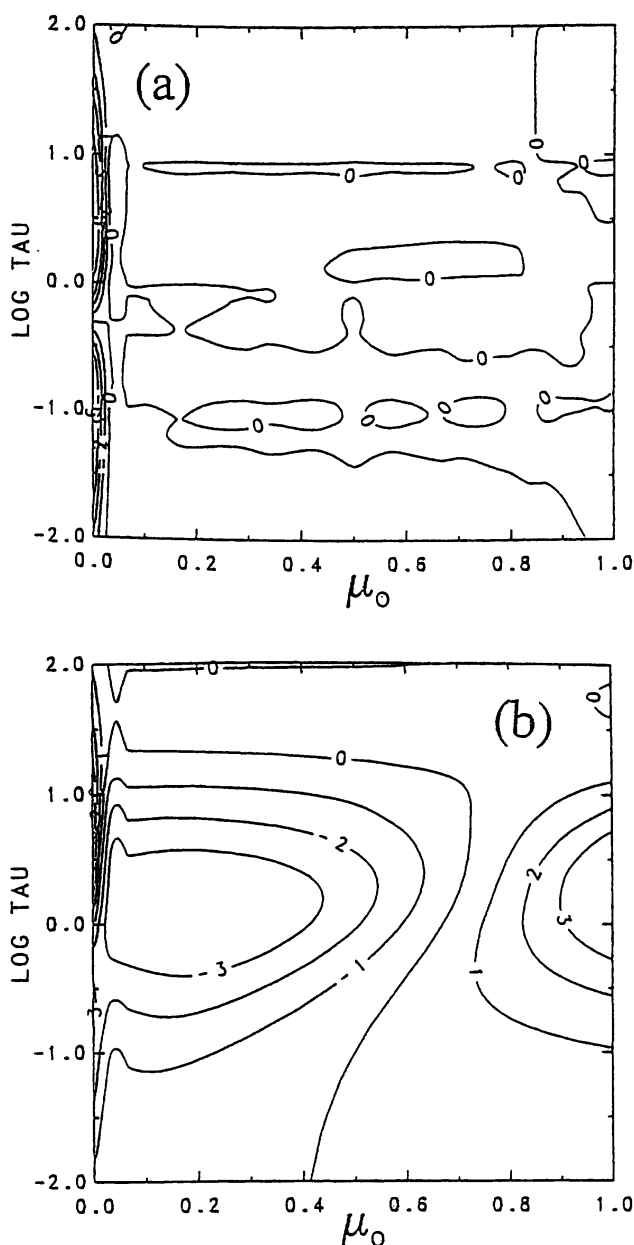


**Figure 1.** Percent albedo error (SGP-DBL)/DBL for (a) isolated cloud and (b) with surface albedo 0.5.

The systematic errors shown in Figure 1b are not easily fixable within the present modeling framework because look-up tables with more than three entries become unwieldy and impractical.

The SGP model is parameterized to provide accurate results for conservative scattering ( $\omega_0 = 1.0$ ) and also for total absorption ( $\omega_0 = 0.0$ ). For intermediate values of  $\omega_0$ , Figure 2a shows that the SGP model overestimates reflection in the case of small optical depths and high sun angles and underestimates layer absorption, but with a somewhat different pattern in  $\tau, \mu_0$  (Figure 2b). For both cases, the surface albedo was zero (higher surface albedos tend to dilute the error). While we could parameterize the SGP model to match the doubling/adding results for any value of  $\omega_0$ , doing so would cause the layer absorbance to be overestimated by an unacceptable amount. As a result, the errors in Figure 2 cannot be readily fixed by simple single-parameter scaling. Because of this, the SGP model tends to underestimate cloud absorption by a small amount, though not by more than a few  $\text{Wm}^{-2}$  in the global GCM context.

## Thermal Radiation

Correlated k-distribution approach is used to merge the narrow-band k-distributions from noncontiguous spectral regions, weighted by Planck spectral radiation (Lacis and Oinas 1991). The absorption coefficients are tabulated as functions of pressure, temperature, and absorber amount for major absorption bands of  $\text{H}_2\text{O}$ ,  $\text{CO}_2$ , and  $\text{O}_3$ . The number of k-intervals was increased from 25 to 33 to more accurately model stratospheric cooling by  $\text{CO}_2$ , and the overlapping absorption by  $\text{H}_2\text{O}$ . As a result, the treatment of the weaker bands of  $\text{H}_2\text{O}$ ,  $\text{CO}_2$ , and  $\text{O}_3$ , and the absorption by  $\text{CH}_4$ ,  $\text{N}_2\text{O}$ , CFC-11 and CFC-12 were also significantly improved. For water vapor continuum absorption, we use the Ma and Tipping (1992) theoretical model.

For cloudy-sky conditions, the thermal fluxes are formally calculated without scattering. A correction for scattering effects for the outgoing radiation is included parametrically via cloud emissivity dependence based on off-line calculations. A 3-point numerical quadrature (for  $\mu = 1.0$ , 0.5, and 0.1), rather than fixed-value diffusivity factor, is used to compute the thermal fluxes. This approach provides better accuracy for top of the atmosphere (TOA) fluxes and stratospheric cooling rates than using a two-stream multiple scattering formulation, while at the same time this approach provides angle dependent radiances for diagnostic purposes and to facilitate more informative comparisons with satellite measurements.

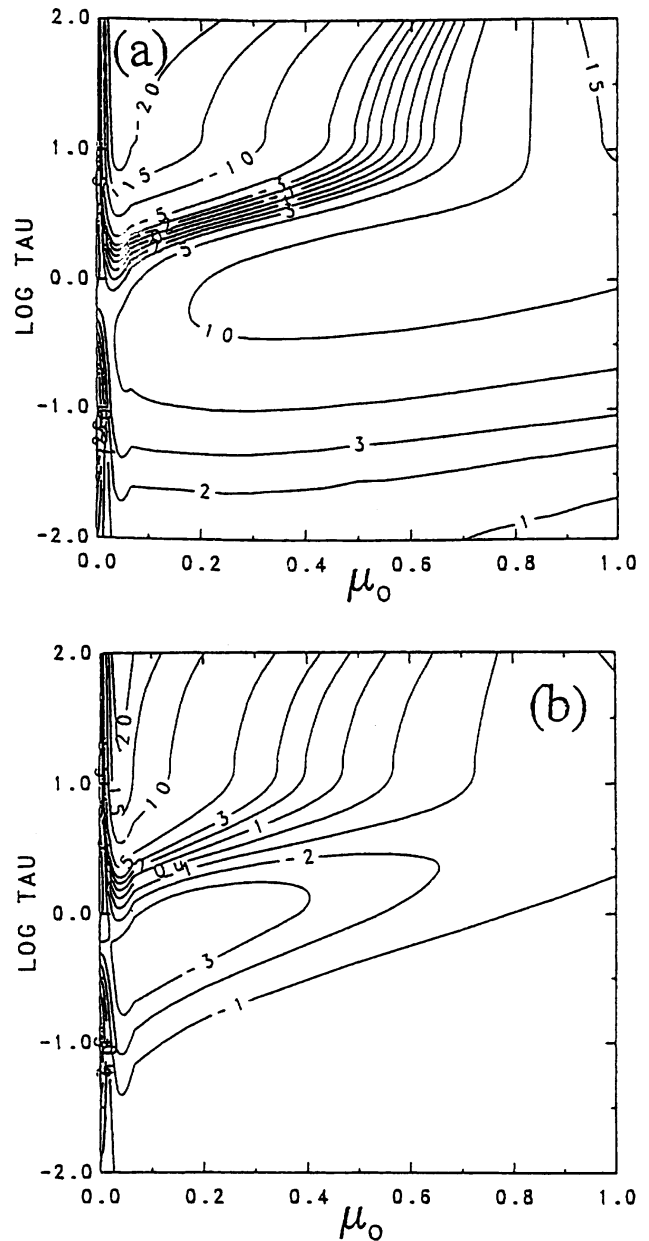


**Figure 2.** Percent albedo error (SGP-DBL)/DBL for (a) albedo and (b) absorbance for  $g = 07$ ,  $\omega_0 = 0.8$ .

## Cloud Radiative Model

For numerical tractability, clouds are taken to be plane-parallel. Cloud cover is fractional in time, and clouds may be single or multilayered. The cloud water content, optical depth, and particle size distribution are set by the prognostic cloud water parameterization (Del Genio et al. 1996),

$$\tau_o = \pi a^2 (1-b)(1-2b) Q_x H N$$

and

$$\text{LWC} = 4/3 \pi a^3 (1-b)(1-2b) \rho H N$$

so that

$$\text{LWC} = 4/3 a \rho \tau_o / Q_x .$$

where,  $a$  is the cloud particle effective radius, and  $b$  is the effective variance of the size distribution,  $Q_x$  is the extinction efficiency factor at  $\lambda = 0.55 \mu\text{m}$ ,  $\rho$  is the mass density,  $H$  is the column height, and  $N$  is the cloud particle number density per unit volume. This defines the (Mie) optical depth,  $\tau_o$ , asymmetry parameter,  $g_o(a)$ , and single scattering albedo,  $\omega_o(a)$ .

Examples of the frequency histogram of the cloud particle effective radius  $a$  ( $\mu\text{m}$ ) occurrence diagnosed in the GCM are shown in Figure 3. Results are January and July accumulations, with left (right) panel showing results for the Northern (Southern) Hemisphere of size histograms for liquid water clouds over ocean (thin line) and over land (bold line), respectively.

The parameterization to model heterogeneous cloud effects (Cairns et al. 1998) is derived from rigorous Monte Carlo modeling simulations for inhomogeneous density distributions. It readily meets the criteria for GCM simplicity in that the plane-parallel homogeneous cloud parameters  $\tau_o, g_o, \omega_o$  are simply re-scaled by the relative variance  $V$  as shown below.

$$\begin{aligned} \tau &= \tau_o / (1 + V) \\ \omega &= \omega_o / [1 + V(1 - \omega_o)] \\ g &= g_o [1 + V(1 - \omega_o)] / [1 + V(1 - \omega_o g_o)] \end{aligned}$$

where

$$V = \exp(\delta^2) - 1$$

and where  $\delta$  is the *log* standard deviation of the droplet density distribution. This formalism provides physical realism for GCM clouds at little extra computing cost.

The principal source of information that determines the cloud radiative effect of subgrid-scale variability is the probability distribution function (PDF) of liquid water path, which can be estimated from the parameters of the Gamma distribution that are provided in the D1 reprocessed version of the International Satellite Cloud Climatology Program (ISCCP) data.

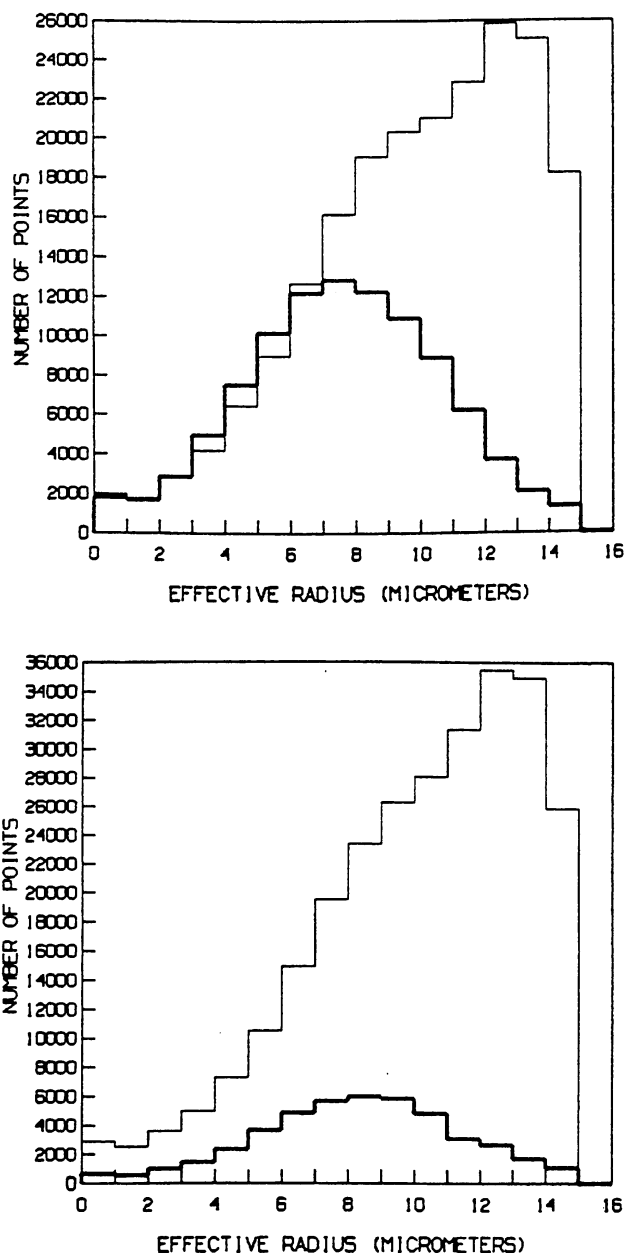


**Figure 3.** GCM-simulated frequency histograms of low cloud liquid droplet effective radius for Northern (top) and Southern (bottom) Hemispheres, assuming uniform but different number concentrations over land (bold line) and ocean (thin line). Results are accumulations over one January and one July time periods.

Figure 4 shows global maps of monthly-mean cloud variability derived from ISCCP D1 data for the cardinal months: January and July 1990 in the upper panels, and April

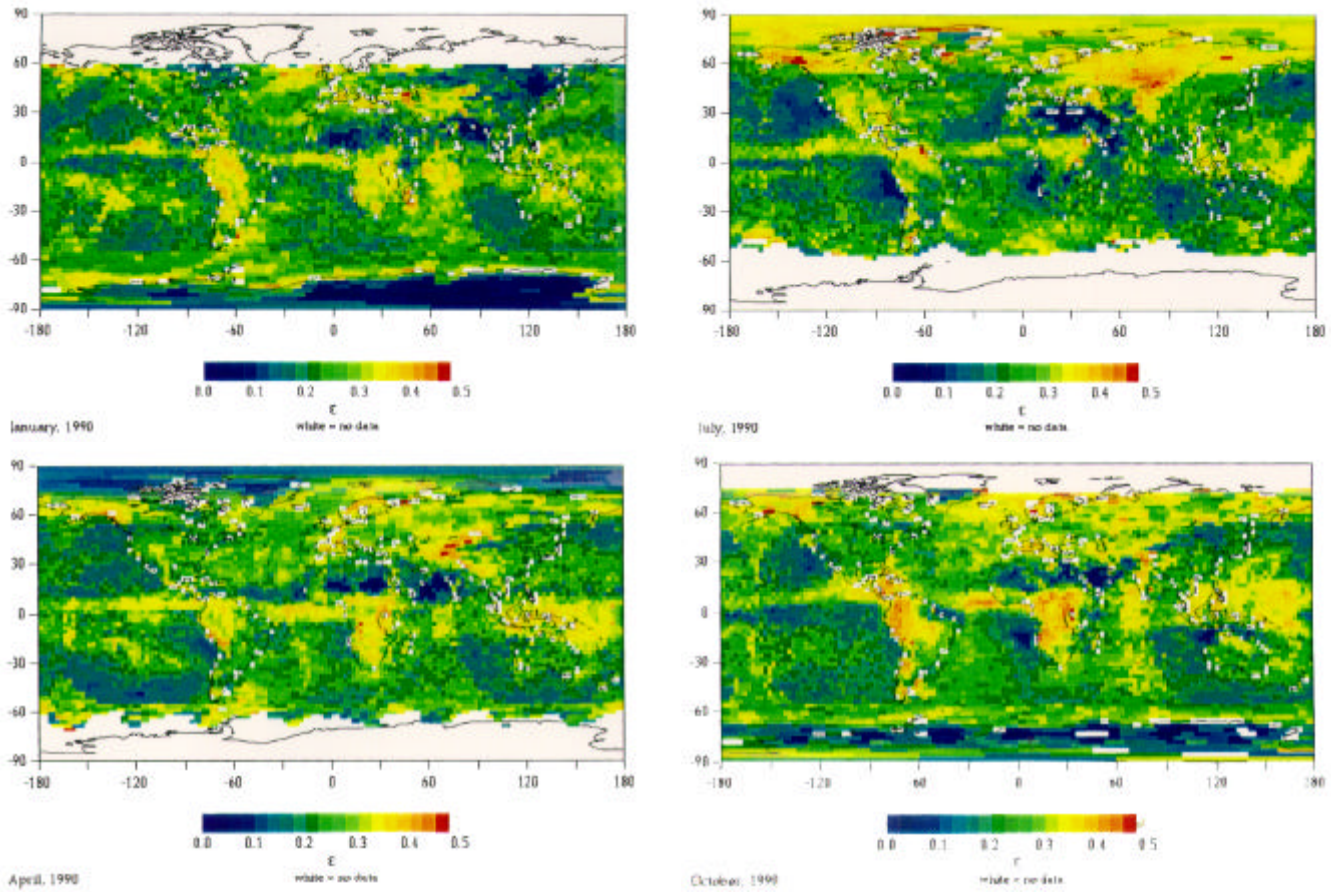


**Figure 4.** Global maps of monthly-mean cloud variability derived from ISCCP D1 data. Upper left panel results are based on January 1990 data; the upper right panel is for July 1990. The bottom panels depict results for April and October 1990, respectively. The quantity plotted is a measure of the relative variability  $\epsilon = V/(1+V)$ . In the deep blue regions where  $\epsilon = 0$ , the homogeneous plane-parallel cloud approximation should be accurate. In the deep red regions where  $\epsilon \approx 0.5$  ( $V \approx 1$ ), the effective optical depth (and liquid water content) differ by a factor of 2 from the homogeneous plane-parallel cloud results. (For a color version of this figure, please see [http://www.arm.gov/docs/documents/technical/conf\\_9803/lacis-98.pdf](http://www.arm.gov/docs/documents/technical/conf_9803/lacis-98.pdf).)

and October in the lower panels, respectively. The quantity plotted  $\epsilon = V/(1+V)$  is a measure of the relative variance of the time-space cloud variability.

Persistently greater cloud variability is evident along the equator. Substantial seasonal changes in variability also occur over continental areas and along the coastal ocean areas. The western Pacific shows greater cloud variability in April and October compared to either in January or July. In the darker regions where  $\epsilon \approx 0$ , the homogeneous plane parallel approximation should be accurate in representing the observed cloudiness. But in the lighter regions where  $\epsilon \approx 0.5$

( $V \approx 1$ ), cloud optical depth and cloud liquid water content can differ by as much as a factor 2 compared to homogeneous plane parallel cloud results.

## References

Cairns, B., A. Lacis, and B. Carlson, 1998: Absorption within inhomogeneous clouds and its parameterization in General Circulation Models. *J. Atmos. Sci.*, in press.

Del Genio, A. D., M.-S. Yao, W. Kovari, and K. W. Lo, 1996: A prognostic cloud water parameterization for global climate models. *J. Climate*, **9**, 270-304.

King, M. D., and Harshvardhan, 1986: Comparative accuracy of selected multiple scattering approximations. *J. Atmos. Sci.*, **43**, 784-801.

Lacis, A. A., and J. E. Hansen, 1974: A parameterization for the absorption of solar radiation in the Earth's atmosphere. *J. Atmos. Sci.*, **31**, 118-133.

Lacis, A. A., and M. I. Mishchenko, 1995: Climate forcing, climate sensitivity, and climate response, in *Aerosol Forcing of Climate*, eds. R. Charlson and J. Heintzenberg, Wiley, Chichester, 11-42.

Lacis, A. A., and V. Oinas, 1991: A description of the correlated k-distribution method for modeling non-grey gaseous absorption, thermal emission, and multiple scattering in vertically inhomogeneous atmospheres. *J. Geophys. Res.*, **96**, 9027-9063.

Ma, Q., and R. H. Tipping, 1992: A far wing line shape theory and its application to the water vibrational bands, II. *J. Chem. Phys.*, **96**, 8655-8663.